Materials Today Sustainability 13 (2021) 100076

Contents lists available at ScienceDirect

Materials Today Sustainability

journal homepage: https://www.journals.elsevier.com/materials-today-sustainability

Tinospora cordifolia extract as an environmentally benign green corrosion inhibitor in acid media: electrochemical, surface morphological, quantum chemical, and statistical investigations

Vidhya Thomas K [a], Joby Thomas K [a, *], Vinod Rapheal P [b], A.S. Sabu [c], K. Ragi [a], Reeja Johnson [a]

[a] Centre for Electrochemical Studies, Department of Chemistry, St. Thomas' College (Autonomous), Thrissur, Kerala 680001, India
[b] Department of Chemistry, Government Engineering College, Thrissur, Kerala, India
[c] Department of Mathematics, St. Thomas' College (Autonomous), Thrissur, Kerala, India

ARTICLE INFO

Article history:
Received 15 March 2021
Received in revised form
7 July 2021
Accepted 10 July 2021
Available online 22 July 2021

Keywords:
Inhibition efficiency
TCE
Mild steel
Tinosponone
Adsorption
EIS
AFM
RSM
BBD

ABSTRACT

The inhibiting capacity of *Tinospora cordifolia* extract (TCE) was evaluated on mild steel in 1 M HCl and 0.5 M H_2SO_4 by physicochemical and electrochemical techniques and by utilizing statistical tools such as response surface methodology and the Box-Behnken design (BBD). Surface properties were ascertained by scanning electron microscopy and atomic force microscopy to confirm the adsorption performance of the inhibitor molecules on the surface of the metal. Experimental results were found to agree with quantum chemical calculations of the active principle of TCE, Tinosponone. Weight loss measurements exhibited extreme inhibition power of TCE as 94.73% and 82.53% in 1 M HCl and 0.5 M H_2SO_4, respectively, at 5 v/v% concentration at 303 K. Electrochemical impedance spectroscopy (EIS) studies were agreed with weight loss measurements as EIS showed an inhibition efficiency of 93.51% in 1 M HCl and 88.68% in 0.5 M H_2SO_4 solutions. Electrochemical studies were evident that TCE can hinder reactions of the cathode and anode of mild steel. Kinetic and thermodynamic studies indicated the mixed-type adsorption behavior of TCE on mild steel by following the Langmuir adsorption isotherm in both acid media. The BBD method was applied to verify the impact of three test factors, temperature, TCE concentration, and acid concentration, on inhibition efficiency of mild steel in HCl medium. Experimental and theoretical results confirmed the anticorrosion potential of the environment-friendly inhibitor TCE.

1. Introduction

In recent years, the regulation of metal corrosion has a great interest in the field of scientific research. Ready availability, notable mechanical strength, and affordable cost make mild steel a widely used alloy in industrial applications. However, the deterioration of mild steel remains a critical issue for the community by considering safety and economic matters. Acid media are used for cleaning purposes of boilers and massive equipment made from mild steel in large-scale production units. However, they cause metal corrosion [1]. Mitigation of metal corrosion during acid treatment requires appropriate acid solutions. Various researchers have been reported that Schiff bases derived from heterocyclic compounds, such as derivatives of imidazole, pyridine, furan, thiophene, and so on, are efficient to protect the metal from corrosion. Still, their high-cost synthesis and hazardous influence on the atmosphere and human beings make them unfriendly inhibitors [2]. The application of extracts from natural products such as leaves, fruits, stems, seeds, and roots as green corrosion inhibitors can overcome the limitations of the synthetic inhibitors. Plant products can adsorb the surface of the metal either by physical or by chemical adsorption [3]. This shielding behavior of the natural products on the metal surface is due to numerous phytochemicals in it, which can interact with the metal surface by donating a lone pair of electrons of heteroatoms and unsaturated and aromatic systems. Thus, the use of eco-friendly corrosion inhibitors has a significant role in chemical research.

For example, *Pimenta dioica* exhibited 86% inhibition potency at a concentration of 400 ppm [4]. Aloe vera exhibited a maximum

* Corresponding author.
E-mail addresses: vidhyathomas@stjosephs.edu.in (V. Thomas K), jobythomask@stthomas.ac.in (J. Thomas K).

https://doi.org/10.1016/j.mtsust.2021.100076
2589-2347/

inhibition power of 88.9% for the mild steel and 99.1% for stainless steel in H_2SO_4 medium [5]. Radish leaf extract also revealed metal protection ability up to 93% at 300 mg/L in 0.5 M H_2SO_4 solution [6]. Pulp of jujube extract exhibited 93% inhibition performance at a concentration of 1 g/L for copper in 1 M HCl medium [7]. Electrochemical studies and the surface morphological studies of low carbon steel revealed 96.62% inhibition performance at 500 mg/L concentration of *Citrus sinensis* [8]. The aqueous extract of Lawsonia leaves showed 95% metal protection ability on carbon steel, nickel, and zinc in acidic, neutral, and basic solutions [9]. *Olea europaea* extract exhibited 93% inhibition potency on carbon steel in 2 M HCl solution [10]. *Eclipta alba* extract showed 99.6% anticorrosion property on mild steel in 1 N HCl [11].

Table 1 introduces some reference works in recent years about plant extracts as corrosion inhibitors [12–21].

It is monotonous to optimize the entire variables under study to acquire a suitable system with improved performance practically. It requires a large number of trials for attaining maximum parameter mixes. This approach is worthless and inconvenient. For this instance, statistical methods and an appropriate design of experiments make it easier to collect data about the optimization setup. Response surface methodology (RSM) is a collaborative method between statistics and mathematics advantageous to the development, refinement, and optimization of process factors and recommends evaluating a combination of a large number of factors with minimum trials. Therefore, it is time- and cost-effective for the optimization of the process. Many researchers have practiced RSM to investigate the impact of various parameters on the system's properties and optimize the test parameters, reducing corrosion rate and elevating the inhibition efficacy. For example, *Terminalia chebula* Ritz. extract showed maximum corrosion inhibition potency of 83.24% with the inhibitor concentration of 500 ppm and H_3PO_4 acid concentration of 0.5 M at 30 °C by RSM, and it was in line with the experimental data [22]. *Garcinia indica* Choisy extract exhibited the highest inhibition capacity of 86.19% with an extract concentration of 0.5g/L in 0.5 M phosphoric acid at 50 °C as optimum conditions by RSM, and it was in good agreement with observed data [23]. The bitter kola leaf extract revealed a maximum inhibition power of 88.24% in the HCl environment by the RSM optimization technique, which matched with electrochemical studies [24].

The point of this perusal is to investigate the applicability of *Tinospora cordifolia* extract (TCE) as an effective environmentally friendly corrosion inhibitor for mild steel in 1 M HCl and 0.5 M H_2SO_4. This work presents corrosion inhibition behavior of the non-toxic and biodegradable inhibitor TCE using modern corrosion analyses such as electrochemical noise spectroscopy and statistical analysis. Although the research world has revealed medicinal characteristics of *Tinospora cordifolia* leaves, their corrosion resistance properties with various competencies are not yet investigated [25]. *Tinospora cordifolia* belongs to the Menispermaceae family. Even though it contains multiple chemical compounds such as berberine, tembetarine, tinocordioside, tinosponone, syringin, magnoflorine, 20-hydroxyecdysone, and so on, the active principle of the *Tinospora cordifolia* leaf is tinosponone [26]. The structure of tinosponone is given in Fig. 1. The presence of myriads of phytochemicals causes antineoplastic, antidiabetic, hypolipidemic, antioxidant, and anti-inflammatory effects. This prompted us to select *Tinospora cordifolia* as a corrosion inhibitor. Acid solution is the widely used aggressive medium for pickling, cleaning, descaling, and oil well acidification. Therefore, we selected HCl and H_2SO_4 as the corrosive medium. Weight loss and electrochemical measurements determined the pace of corrosion on mild steel with various concentrations of TCE at room temperature. In addition, the synergistic effects of TCE concentration, acid concentration, and temperature on the corrosion inhibition potency were evaluated using RSM and surveyed with critical statistical tools.

2. Experimental method

2.1. Preparation of TCE

Leaves of *Tinospora cordifolia* were washed, withered at room temperature, and ground to a fine powder. Five grams of powder was weighed and refluxed for 4 h in 100 ml ethanol. It was filtered and concentrated to 50 ml by staying overnight. The concentrations made for the analysis were 1–5 v/v%.

2.2. Preparation of mild steel coupons

Weight percentage of the mild steel used was as follows: carbon—2.95% and iron—97.05%. A mild steel metal sheet was cut into 1 cm^2 area coupons, and then they were smoothened using different grades of abrasive material, such as 100, 220, 440, 800, 1,000, 1,500, and 2,000, and cleaned with distilled water and acetone.

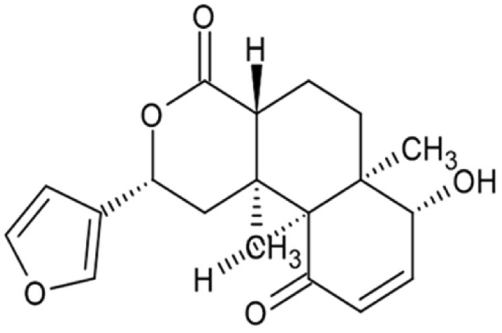

Fig. 1. Structure of tinosponone.

Table 1
Some reference works of plant extracts in recent years.

Extracts	Metal	Medium	Inhibition efficiency	Year
Eucalyptus leaf	Mild steel	0.5 M H_2SO_4 and H_3PO_4	91% (0.4 mol/L)	2020
Rosa canina fruit	Mild steel	1 M HCl	80.5% (800 ppm)	2019
Ficus tikoua leaves	Carbon steel	1 M HCl	93.8% (100 mg/L)	2019
Mangifera indica	Mild steel	1 M HCl	92% (1,000 ppm)	2019
Esfand seed	Low-carbon steel	NaCl solution	98.8% (300 ppm)	2020
Rice straw	Low-carbon steel	3.5% NaCl	92% (1.5 g/L)	2019
Papaya leaves	Copper	0.5 M H_2SO_4	95.5% (150 mg/L)	2021
Papaver somniferum	Mild steel	1 M HCl	97.64% (600 ppm)	2020
Citrullus lanatus fruit	Mild steel	1 M HCl	91% (800 ppm)	2019
Juglans regia green fruit shell	Mild steel	3.5% NaCl	94% (1,000 ppm)	2019

2.3. Preparation of acidic media

Analytical pure (Merck) HCl and H_2SO_4 were used for preparing 1 M HCl and 0.5 M H_2SO_4. The volume of acidic media was 50 ml for weight loss measurements. The influence of temperature on the rate of corrosion was analyzed at various temperatures, 303 K, 313 K, 323 K, and 333 K.

2.4. FTIR spectroscopy

The IR spectrum of TCE was examined using the Shimadzu IR Affinity-1 model FT-IR spectrophotometer.

2.5. Weight loss measurement

Weight loss corrosion studies were conducted with and without 1–5 v/v% concentrations of TCE in both acid solutions for a 24-h immersion period at different temperatures. Smoothened mild steel coupons were pre-measured, pre-weighed, and immersed in 1 M HCl and 0.5 M H_2SO_4 solutions separately, adding 0–5 v/v% concentrations of TCE. TCE was observed to be soluble in both acids. After the completion of the period of immersion, metal coupons were weighed and their weight loss was calculated. Equation (1) is used to find out the corrosion rate (υ) of mild steel [27]:

$$\upsilon = \frac{KW}{DSt} \tag{1}$$

where K = 87,600, W is the weight loss of metal coupon (g), S is the total area of the coupon (cm^2), D is the density of metal (g/cm^3), and t is the period of immersion (h). Percentage of the mitigation potential of TCE was calculated from the values of υ, using equation (2) [28]:

$$\eta\% = \frac{\upsilon_0 - \upsilon}{\upsilon_0} \times 100 \tag{2}$$

where υ_0 and υ denote the pace of corrosion of metal coupons immersed in acid media without and with the inhibitor TCE, respectively.

2.6. Electrochemical studies

Electrochemical impedance spectroscopy (EIS), polarization studies, and electrochemical noise studies were performed using the Ivium CompactStat electrochemical workstation and IviumSoft software by using a three-electrode electrochemical cell. For all the electrochemical studies, a saturated calomel electrode behaved as the reference electrode. For EIS and linear polarization studies, a platinum electrode acted as the counter electrode, and the mild steel having 1 cm^2 exposed surface area was used as a working electrode. Two mild steel samples with 1 cm^2 exposed surface area were utilized as counter and working electrodes in electrochemical noise studies. The measurements were carried out at room temperature using 1 M HCl and 0.5 M H_2SO_4 with various concentrations (1–5 v/v%) of TCE.

EIS parameters were measured over a frequency span of 1 KHz to 100 mHz and 10 mV signal breadth. Corrosion inhibition power of TCE was calculated from R_{ct} values obtained from Nyquist plots by equation (3) [29].

$$\eta_{EIS}\% = \frac{R'_{ct} - R_{ct}}{R'_{ct}} \times 100 \tag{3}$$

R'ct and Rct represent the working electrode's charge transfer resistance with and without the inhibitor TCE, respectively.

Current-potential relationship of mild steel samples in the test solution was evaluated by potentiodynamic polarization studies using the open-circuit potential method. The applied potential range for the working electrode was from −250 to +250 mV compared with the corrosion potential (E_{corr}) with a scan rate of 1 mV/s. Surveillance of anodic and cathodic curves was accomplished to obtain corrosion current density (i_{corr}), which was used to derive the percentage of inhibition potency (η_{pol}%) as in equation (4) [30].

$$\eta_{pol}\% = \frac{i_{corr} - i'_{corr}}{i_{corr}} \times 100 \tag{4}$$

i_{corr} and i'_{corr} indicate the corrosion current densities of the working electrode in the absence and presence of the inhibitor TCE, respectively.

Inhibition efficiency (IE) also can be calculated from linear polarization parameters using the following equation (5):

$$\eta_{Rp}\% = \frac{R'_p - R_p}{R'_p} \times 100 \tag{5}$$

where R'_p and R_p are polarization resistance in the presence and absence of the inhibitor TCE, respectively.

Electrochemical noise studies were carried out for the period of 1200s.

2.7. Surface morphological studies

Surface characterization of mild steel coupons submerged in 1 M HCl and 0.5 M H_2SO_4 media comprising 5 v/v% of TCE was examined by scanning electron microscopy (SEM) (JEOL Model J.S.M.-6390LV) and atomic force microscopy (AFM) (WITEC ALPHA300 RA). The immersion period for the mild steel in contact with acid media and TCE was 24 h.

2.8. Quantum chemical calculations

Molecular structure of the inhibitor has a crucial role in the determination of corrosion inhibition potency. The mechanism of corrosion resistance can be demonstrated concerning HOMO-LUMO interaction between filled orbitals of inhibitor molecules and vacant orbitals of Fe. Lower change in energy value ($\Delta E = E_{LUMO} - E_{HOMO}$) is the benchmark for solid adsorption of inhibitor molecules on the metal surface [31]. The quantum chemical parameters of tinosponone, an active TCE principle, were calculated using the Density functional theory (DFT) method by GAMMES software. The correlation factor used was B3LYP and STO-3G as the basis set.

Monte Carlo simulation is used to attain stable adsorption sites on metal surfaces with low-energy adsorption sites on both periodic and non-periodic substrates. Materials Studio 17.1 software from Accelrys, Inc. has been applied to simulate the adsorption of tinosponone and its protonated form on the Fe (110) plane. Because of the higher stability of Fe (110) than the Fe (1 00) and Fe (111) plane, it was adopted for the simulation studies. Optimized structures of tinosponone, protonated form, and the Fe surface were used for this study. As per the Accelrys website, the Forcite module can be defined as an advanced classical molecular mechanics tool in which energy calculations are rapid, and geometry optimization is well-founded. Optimization of Fe surface and inhibitor molecules was performed by the forcefield COMPASS (condensed-phase optimized molecular potentials for atomistic simulation studies). Solvent and charge effects were ignored, and the simulations were carried out at the metal/vacuum interface. The following equation

(6) gives the binding energy between tinosponone and Fe (110) surface [32].

$$E_{binding} = E_{total} - \left(E_{surface} + E_{inhibitor}\right) \quad (6)$$

where E_{total} is the total energies of the Fe (1 1 0) surface when tinosponone adsorbed on it, $E_{surface}$ indicates the energy of $Fe_{surface}$, and $E_{inhibitor}$ corresponds to the energy of tinosponone molecules. A stable adsorption system implies the negative value of $E_{binding}$.

2.9. Response surface methodology

RSM is the established optimization technique in current years. It describes the effect of a quantitative response on process factors, individually or with one another, and generates an empirical model illustrating the proper quantity of processes [33]. It helps to discover the optimum parameter condition to attain the maximum IE. Experimental design and analysis were performed using Minitab 19 programming tool, and the Box-Behnken design (BBD) was applied to include 15 experimental runs. Three factors were incorporated: X_1—temperature (K), X_2—TCE concentration (v/v%), and X_3—acid concentration, at three levels, as shown in Table 2. The generalized full quadratic response for the three factors X_1, X_2, and X_3 in the RSM is shown in equation (7).

$$Y = a_0 + a_1X_1 + a_2X_2 + a_3X_3 + a_{12}X_1X_2 + a_{13}X_1X_3 + a_{23}X_2X_3 + a_{11}X_1^2 + a_{22}X_2^2 + a_{33}X_3^2 \quad (7)$$

where Y is the predicted values of corrosion IE. a_0 is a constant, a_1, a_2, and a_3 are constants indicating the effect of factors X_1, X_2, and X_3, respectively. a_{12}, a_{13}, and a_{23} are interaction constants between the two factors X_1X_2, X_1X_3, and X_2X_3, respectively. a_{11}, a_{22}, and a_{33} represent quadratic constants of X_1, X_2, and X_3, respectively.

3. Results and discussions

3.1. FTIR spectroscopy

The Fourier transform infrared spectroscopy (FTIR) spectrum of TCE revealed characteristic stretching and bending frequencies for various bonds, drawn in Fig. S1. The broadband at 3,277 per cm denotes O–H stretching. Two sharp bands at 2,917 per cm and 2,849 per cm represent alkyl C–H stretching vibrations. A >C=O stretching vibration appears at 1,736 per cm. This peak can be assigned to six-membered cyclic lactones. The bands at 1,318 per cm and 1,603 per cm can be accredited to C=C and aromatic C=C stretching vibrations. The C–O bending pulse appears as a weak band at 1,231 per cm and 1,016 per cm. This peak can be ascribed to characteristic peaks for the furan ring. The band at 750–620 per cm corresponds to aromatic substitutions. In summary, distinct peaks of TCE can be attributed to various phytochemicals involving heteroatoms, aromatic rings, and unsaturated compounds.

Table 2
The level of factors of the BBD with coded and uncoded form.

Sl. No.	Factor	Code	Unit	Level of factors		
				Low (−1)	Center (0)	High (1)
1	Temperature	X_1	K	313	323	333
2	TCE concentration	X_2	v/v%	1	3	5
3	Acid concentration	X_3	M	0.5	1	1.5

3.2. Weight loss measurements

3.2.1. Effect of TCE concentration

Corrosion IE (η%) and corrosion rate (υ) found by weight loss technique on mild steel in 1 M HCl and 0.5 M H_2SO_4 with varying concentrations (0–5 v/v%) of TCE have been calculated (Table 3).

An augment in inhibition power was noticed from the data by raising TCE concentration in both acid media. Also seen that TCE behaves as an efficient green corrosion inhibitor in 1 M HCl, attaining maximum inhibition efficacy of 94.73% and 82.53% in 0.5 M H_2SO_4 at 5% TCE concentration. In HCl solution, TCE exhibits more inhibition capacity compared with H_2SO_4 solution. It may be due to the effective adsorption of Cl^- ions on the metal surface than SO_4^{2-} ions because halide ions are more electronegative. It may lead to more adsorption of cationic organic molecules on the metal surface to inhibit metal dissolution. At the same time, SO_4^{2-} the fraction of TCE molecules adsorbed on mild steel surface is low, and hence, metal suffers a high corrosion rate in the H_2SO_4 medium. All experiments were conducted three times to maintain reproducibility.

Evaluation and statistical analysis of weight loss measurement are essential in determining the precision of corrosion rate. Table 3 shows that the mean values are close, which means that weight loss measures are in the same acceptance. Similarly, the standard deviation (σ) of the inhibitory efficiency indicates that the observed corrosion rates in triplicate experiments are in good agreement.

Comparing the IE of TCE with reported extracts, TCE shows tremendously good results. A Dehghani et al. [34] said that *Laurus nobilis* extract showed 92% inhibition ability on carbon steel in 1 M HCl for 400 ppm concentration of extract. Siyi Chen et al. [35] discovered that coconut leaf extract inhibited 91.7% corrosion on X60 steel in 1 M HCl using 400 mg/L of the extract. Shujun chen et al. [36] pointed out that *Magnolia grandiflora* extract acted as a corrosion inhibitor for Q235 steel in 1 M HCl with 85% inhibition performance at 500 mg/L of the extract. Camphor leaves were proved to have 89.4% inhibition power on Q235 steel in 1 M HCl with 600 mg/L inhibitor concentration by Huajun Zhao et al. [37]. TCE exhibited improved IE (94.73%) in 1 M HCl than all these recently cited works.

3.2.2. Adsorption isotherms

Adsorption isotherm studies provide an interaction mechanism between inhibitor molecules and mild steel. Among different adsorption isotherm models, such as Langmuir, El-Awady, Frumkin, Temkin, Freundlich, Flory-Huggins isotherms, the best adsorption isotherm model of TCE in 1 M HCl and 0.5 M H_2SO_4 was explored by fitting the extent of surface coverage (θ) and corrosion rate into it. The Langmuir adsorption isotherm was found to be the best model with an R^2 value of 0.9987 and 0.9974 in 1 M HCl and 0.5 M H_2SO_4, respectively. The Langmuir isotherm is represented as in equation (8) [38].

$$\frac{C}{\theta} = \frac{1}{K_{ads}} + c \quad (8)$$

where θ is the extent of occupancy of adsorbed sites, C signifies the inhibitor's concentration, and K_{ads} implies the adsorption equilibrium constant.

Standard free energy of adsorption ΔG^0_{ads} can be calculated from the adsorption equilibrium constant K_{ads} as in equation (9) [39].

Table 3
Corrosion rate and inhibition efficiency of TCE in 1 M HCl and 0.5 M H_2SO_4 at room temperature for 24 h.

Acid	Conc. (v/v%)	Corrosion rate (mm/yr)				Variance (σ^2)	Standard deviation (σ)	Inhibition efficiency (%η)
		x_1	x_2	x_3	Mean X			
1 M HCl	Blank	3.85	3.71	4.29	3.9500	0.061066	0.2471	–
	1	0.7852	0.6940	0.8764	0.7852	0.005544	0.0744	80.12
	2	0.5727	0.5532	0.5934	0.5731	0.000269	0.0164	85.49
	3	0.453	0.4230	0.4830	0.4530	0.000600	0.0244	88.53
	4	0.3365	0.2930	0.3800	0.3365	0.001261	0.0355	91.48
	5	0.2081	0.2137	0.2025	0.2081	0.0000209	0.0045	94.73
0.5 M H_2SO_4	Blank	33.97	35.37	37.37	35.57	1.946666	1.3952	–
	1	16.851	19.117	17.321	17.76	0.953474	0.9764	50.06
	2	13.25	12.08	14.78	13.37	1.222200	1.1055	62.41
	3	10.756	7.246	9.112	9.038	2.056088	1.4339	74.59
	4	6.482	7.741	8.376	7.533	0.6195046	0.7870	78.82
	5	6.978	6.550	5.114	6.214	0.6355306	0.7972	82.53

$$\Delta G^0_{ads} = -RT\ln(55.5K_{ads}) \quad (9)$$

where 55.5 suggests the molar concentration of water; R and T point out universal gas constant and the temperature in K, respectively. It was reported that ΔG^0_{ads} values within −20 kJ/mol and −40 kJ/mol showed a mixed-type adsorption mechanism by TCE molecules [40]. In the present work, ΔG^0_{ads} values for TCE−mild steel adsorptions were −30.37 and −27.15 kJ/mol in 1 M HCl and 0.5 M H_2SO_4, respectively, which showed the nature of adsorption was both physisorption and chemisorption. Fig. S2 represents Langmuir adsorption isotherms of TCE on mild steel in 1 M HCl and 0.5 M H_2SO_4 at room temperature. Fig. 2 portrays the possible surface behavior of TCE molecules on mild steel. Even though TCE contains various components, the principal component is regarded as an authoritative compound for corrosion inhibition. The effective adsorption of tinosponone molecules by donating electrons from oxygen atoms in the furan ring, −OH, lactone functional groups, and π-electrons in the aromatic system causes the formation of a protective film on the metal surface and thereby mitigates metal corrosion. Moreover, tinosponone molecules may interact via back donation of d electrons from the metal to π* orbitals of tinosponone molecules. Besides this interaction, physisorption of TCE molecules was involved. Initially, chloride/sulfate ions present in the acid solution approach on the surface of mild steel and continue as a cathode. The cationic molecules of TCE, which are considerably larger than acid ions, were adsorbed on the metal surface by the substitutional adsorption process. It caused interference in the anodic and cathodic process of metal corrosion and decreased metal dissolution rate.

3.2.3. *Effect of temperature*

Stability of the protective film of TCE by adsorption on mild steel surface was described by performing temperature studies [32].

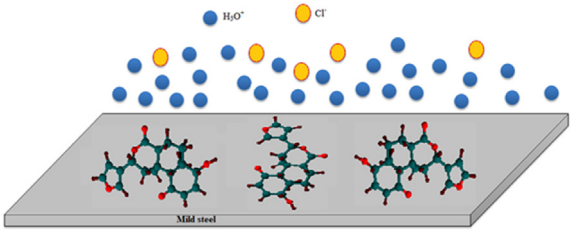

Fig. 2. Interaction diagram of tinosponone molecules with mild steel.

Here, the impact of temperature on the corrosion control was accomplished by weight loss measurements in 1 M HCl and 0.5 M H_2SO_4 with varying TCE concentrations at different temperatures (303−333 K) for 24 h. Inhibition potential was calculated and given in Table 4 and is graphically depicted in Fig. 3. It showed that the rate of corrosion rises with an enhancement in temperature for a fixed concentration. It may be ascribed to the metal surface changes such as instant engraving, crack, detachment of adsorbed film, decay, or reordering of the inhibitor when the temperature rises and thereby decreases inhibition potency. Therefore, discrepancies in temperature influence the metal disintegration, action of the inhibitor, either adsorption or desorption, and corrosion control.

The Arrhenius-type equation can be used to attain activation energy of corrosion as in equation (10) [41].

$$K = A\,e^{(-E_a RT)} \quad (10)$$

K signifies the rate of corrosion, and A is assigned for the pre-exponential factor. E_a specifies the activation energy for decay, R suggests universal gas constant, and T indicates Kelvin's temperature.

Fig. S3a and S4a exhibit Arrhenius plots of log K vs. 1/T for metal corrosion in the presence and absence of TCE in acid media.

Slopes of the plots were fit to evaluate the activation energy of corrosion in acid media. Thermodynamic parameters such as enthalpy (ΔH*) and entropy (ΔS*) were estimated using transition state theory as in equation (11) [42].

$$K = \left(\frac{RT}{Nh}\right)\exp\left(\frac{\Delta S^*}{R}\right)\exp\left(\frac{-\Delta H^*}{RT}\right) \quad (11)$$

where N represents the Avogadro number, and h is Planck's constant. Slopes of the Arrhenius plots of log K/T vs. 1/T (Fig. S3b and S4b) give ΔH* and ΔS* values. All these thermodynamic parameters were tabulated in Table 5, which establishes that the activation energy of corrosion increases with an increase in TCE concentration owing to the growing energy barrier. It also emphasizes an activation complex compound formed by the interaction between the inhibitor and mild steel [43]. The positive value of enthalpy describes the endothermic character of the metal corrosion process [44]. The values of ΔS^* were also increased by adding TCE concentration. Negative values of the entropy of activation for corrosion in the absence of TCE mention a decrease in randomness for the activated complex than the reactants [45]. Disorderliness of the activated complex increases as the concentration of TCE raises and ΔS^* possessed positive values.

Table 4
Corrosion rate (υ) in mm/yr and inhibition efficiency (% η) of TCE in 1 M HCl and 0.5 M H_2SO_4 at different ranges of temperatures for 24 h.

Media	Conc. (v/v%)	υ (303 K)	% η (303 K)	υ (313 K)	% η (313 K)	υ (323 K)	% η (323 K)	υ (333 K)	% η (333 K)
1 M HCl	Blank	3.95	–	13.11		22.05	–	31.77	–
	1	0.7852	80.12	5.23	60.11	13.54	38.61	20.48	35.54
	2	0.5731	85.49	4.72	64.00	10.69	51.53	17.36	45.36
	3	0.4530	88.53	2.15	83.60	8.23	62.68	14.69	53.76
	4	0.3365	91.48	2.07	84.21	7.45	66.22	12.98	59.14
	5	0.2081	94.73	1.26	90.39	6.15	72.11	11.87	62.64
0.5 M H_2SO_4	Blank	35.57	–	58.27	–	86.25	–	106.2	–
	1	17.76	50.06	29.69	49.04	44.95	47.88	60.04	43.49
	2	13.37	62.41	23.08	60.39	36.58	57.58	51.64	51.40
	3	9.03	74.59	19.36	66.77	31.95	62.95	45.91	56.79
	4	7.53	78.82	12.88	77.89	27.23	68.42	40.12	62.24
	5	6.21	82.53	10.77	81.51	20.14	76.64	35.48	66.61

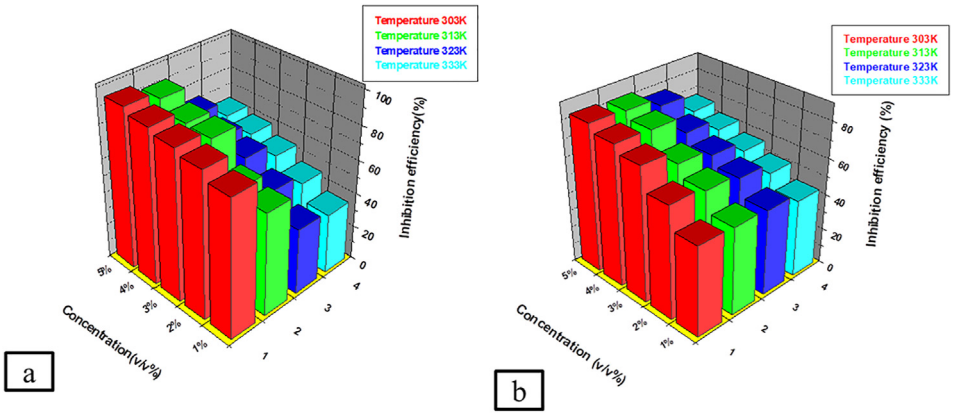

Fig. 3. Variation in inhibition efficiency of TCE in (a) 1 M HCl and (b) 0.5 M H_2SO_4 at elevated temperatures.

Table 5
Thermodynamic parameters of mild steel corrosion with and without TCE in 1 M HCl and 0.5 M H_2SO_4.

Medium	Conc. (v/v%)	E_a (kJ/mol)	A	ΔH* (kJ/mol)	ΔS* (J/mol/K)
1 M	Blank	57.24	3.58×10^{10}	54.6	−44.7842
HCl	1	90.79	4.95×10^{15}	88.15	53.66
	2	93.51	1.13×10^{16}	90.87	60.51
	3	99.28	6.98×10^{16}	96.64	75.66
	4	103.28	2.76×10^{17}	100.64	87.09
	5	115.60	2.14×10^{19}	112.97	123.27
0.5 M	Blank	30.96	8.16×10^{6}	28.3	−114.510
H_2SO_4	1	34.23	1.47×10^{7}	31.59	−109.622
	2	37.95	4.82×10^{7}	35.31	−99.744
	3	45.29	6.31×10^{8}	42.65	−78.349
	4	48.42	1.66×10^{9}	45.78	−70.332
	5	49.06	1.73×10^{9}	46.42	−69.974

3.3. Electrochemical studies

3.3.1. Open-circuit potential (OCP) curves

The OCP of the mild steel electrode was analyzed at the beginning of electrochemical measurements for 20 min to attain a steady-state condition. It was conducted in acid media with and without various concentrations of TCE. OCP vs. time plots (Fig. S5) exhibited that the permitted time was apparent for the corrosion system to become stable. The OCP shift to a positive potential in the presence of TCE pointed out the existence of a durable and protective layer formed by TCE on the mild steel surface [46].

3.3.2. Electrochemical impedance spectroscopy

The corrosion response of mild steel in 1 M HCl and 0.5 M H_2SO_4 solutions with various concentrations of TCE (0–5 v/v%) was demonstrated using EIS at 30^0c. In the present investigation, Randle's circuit was used as an equivalent circuit (Fig. S6), including solution resistance R_s, charge transfer resistance R_{ct}, and double-layer capacitance C_{dl}. Equivalent circuit fitting curves for mild steel with 1% TCE in both media are shown in Fig. S7. The deviations from the metal surface's ideal dielectric behavior lead to a constant phase element (CPE) instead of C_{dl} [47].

$$Z_{CPE} = Q^{-1}(j\omega)^{-n} \quad (12)$$

Q is the extent of the CPE, n is the exponent of the value of the CPE, ω represents the angular frequency, and j is the imaginary number.

Fig. 4 and S8 show Nyquist plots and Bode plots, respectively. Nyquist plots are in a depressed semicircular shape with an

Table 6
Impedance data for mild steel in 1 M HCl and 0.5 M H_2SO_4 with and without various concentrations of TCE.

Conc. (v/v%)	1 M HCl			0.5 M H_2SO_4		
	$R_{ct}(\Omega cm^2)$	$C_{dl}(\mu Fcm^{-2})$	$\eta_{EIS}\%$	$R_{ct}(\Omega cm^2)$	$C_{dl}(\mu Fcm^{-2})$	$\eta_{EIS}\%$
Blank	15.7	78.75	-	18.1	47.39	-
1	74.5	62.8	78.92	37.3	46.5	51.47
2	125	48.9	87.44	41.3	44.1	56.17
3	153	47.5	89.73	86.3	39.0	79.02
4	174	45.6	90.97	100	40.3	81.9
5	242	42.1	93.51	160	32.6	88.68

inhibitor. It can be interpreted as the result of surface in-homogeneity. The adsorption phenomenon on the surface or development of the porous or non-porous passivation layer on coating is the root cause for surface in-homogeneity [48]. The Nyquist plots evinced a single capacitive loop for each concentration. It may be due to the occurrence of a charge transfer reaction at the electrode/solution interface. On examining the plots, it can be seen that the diameter of the semicircle increases by the addition of TCE concentration. Table 6 clearly showed that R_{ct} values are directly proportional to TCE concentration, indicating that the mild steel corrosion is mitigated by the inhibitor TCE. Conversely, C_{dl} values decreased by the addition of TCE. This is due to a drop in the dielectric constant or rise in the thickness of the electrical double layer. It recommends the formation of an interfacial protective layer between metal and acid [4]. Moreover, decreasing tendency of C_{dl} values may be ascribed to the adsorption of TCE molecules on the metal surface by replacing water molecules, favoring the prevention of metal dissolution [49]. Bode plots displayed that as the concentration of TCE increases, the peak size also increases. It may be accounted for the lower capacitive behavior of mild steel, indicating adsorption of TCE molecules on the metal surface [50]. IE of TCE attained 93.51% in 1 M HCl and 88.68% in 0.5 M H_2SO_4 for the highest concentration under supervision. EIS results were also supplemented with the weight loss measurements.

3.3.3. Potentiodynamic polarization studies

Potentiodynamic polarization studies on mild steel were carried out to evaluate the protective ability of TCE on the surface of mild steel in 1 M HCl and 0.5 M H_2SO_4. Fig. 5 and S9 exhibit Tafel and linear polarization plots, and Table 7 reveals polarization parameters such as corrosion current densities (i_{corr}), corrosion potential (E_{corr}), cathodic Tafel slope (b_c), anodic Tafel slope (b_a), and polarization resistance (R_p). On close observation to the table as mentioned previously, it is clear that there was a remarkable decrease in i_{corr} values when TCE concentration increased and inhibition efficacy was found to be boosted. It can be indicated that there is strong resistance in the corrosion process [51]. It can be explained that the cathodic and anodic processes are being prevented by the adsorption of TCE molecules on the mild steel surface. Anodic dissolution of iron is an anodic corrosion process, whereas cathodic evolution of hydrogen is the cathodic corrosion process. The following equations can express both approaches.

$$Fe_{(s)} \rightarrow Fe^{2+}_{(aq)} + 2e^- \quad (13)$$

$$2H^+_{(aq)} + 2e^- \rightarrow H_{2(g)} \quad (14)$$

The sharp decrease in the anodic and cathodic current density, suggesting the adsorption layer formation on the mild steel surface by TCE, retards anodic and cathodic reaction rates. There was a noticeable decrease in current density on increasing TCE concentration, implying good inhibition from the metal corrosion [46].

The mechanism of electrochemical inhibition can be demonstrated as the interaction between partially dissolved iron cations and TCE molecules. The protonated TCE molecules could physically adsorb on the anodic sites of the metal surface through negatively charged chloride and sulfate ions. TCE molecules can chemically adsorb on the mild steel surface too. The unoccupied d orbital of iron cations can accept the lone pair of electrons from the heteroatoms in TCE molecules. It leads to the deposition of protective film on the anodic sites of mild steel. Furthermore, TCE molecules can adsorb on the cathodic sites of the metal by the involvement in the interaction of π-electrons of the aromatic ring and unsaturated bonds of TCE molecules with the vacant d orbitals of iron. The smallest i_{corr} value was reached at the highest TCE concentration under study. These observations could reveal high potency in mild steel corrosion rate diminution by adsorption and/or a protective layer formed on the active sites of the mild steel surface.

The increase in TCE concentration can reason the measured E_{corr} value shift toward less negative values that cause the corrosion prevention effect of TCE. It was reported that if the E_{corr} value shift from the blank is within ±85 mV, such an inhibitor can be regarded

Table 7
Potentiodynamic polarization data of mild steel with and without TCE in 1 M HCl and 0.5 M H_2SO_4.

Media	Tafel data						Polarization data	
	Conc. (v/v%)	$-E_{corr}$ (mV/SCE)	i_{corr} ($\mu A/cm^2$)	−bc (mV/dec)	ba (mV/dec)	$\%\eta_{pol}$	Rp (ohm)	$\%\eta_{Rp}$
1 M HCl	Blank	597.9	1,240	221	166	–	33.14	–
	1	589.5	190.9	151	94	84.60	131.9	75.28
	2	586.9	105.1	176	91	91.52419355	228.9	85.5
	3	573.4	103.5	149	86	91.65	248.5	86.66
	4	572.6	82.12	132	85	93.35	273.9	87.90
	5	568.5	71.62	159	82	94.22	328.4	89.90
0.5 M H_2SO_4	Blank	602.2	161.6	193	184	–	25.3	–
	1	562.8	845.2	184	210	46.70	50.35	49.75
	2	595.9	507.1	161	210	67.62	72.14	64.92
	3	599.6	445.1	137	199	71.46	78.24	67.66
	4	529.6	435.6	173	124	72.05	79.14	68.03
	5	601.5	388.0	143	194	75.00	92.12	72.53

as a mixed-type inhibitor [16]. Herein, the shift in E_{corr} values varies from 1 mV to 72 mV for both acid media toward less negative values. It reflects the mixed-type inhibition character of TCE. The higher inhibition power on mild steel surface was displayed by 5% TCE concentration in HCl and H_2SO_4 media as 94.22% and 75%, respectively. A lower efficiency in H_2SO_4 than HCl medium was observed, similar to the weight loss and EIS studies. From Tafel plots, both cathodic and anodic Tafel slopes change appreciably in the presence of TCE, further suggesting that TCE acts as a mixed-type inhibitor.

The linear polarization plot is another form of the Tafel plot. R_p values were derived from the slope of linear polarization plots. On analyzing Table 7, it was apparent that as the concentration of TCE increases, R_p values were also raised. This trend reflects the adsorption of TCE molecules on the metal surface. Inhibition efficiencies estimated from R_p values have agreed with weight loss and EIS studies.

3.3.4. Electrochemical noise studies

Fig. 6 reveals the current noise for mild steel dipped in 1 M HCl and 0.5 M H_2SO_4 solutions containing various TCE concentrations (0, 1, 3, 5 v/v%). On inspection of the figure, it was evident that the current noise for inhibited metal has a low value compared with uninhibited metal, which implies that TCE possesses considerable IE. As concentration increases, the value of current noise lowered. The signal was at a higher magnitude for the blank experiment, indicating mild steel surface undergoes localized corrosion [52].

Power spectral density (PSD) plots for inhibited and uninhibited metal in acid media are shown in Fig. S10. As frequency increases, current noise lowered. It exhibited magnitudes of current noise relatively large for the metal dipped in acid solution without TCE than the metal immersed in acid solution with TCE. It specified metal corrosion can be inhibited using TCE.

Pitting index is an assessment of the degree of resistance power to pitting corrosion [53]. Fig. S11 shows pitting index curves for mild steel immersed in the absence and presence of various TCE concentrations. It was clear that as the concentration of TCE increases, the pitting index value rises. The HCl pitting index value was 6 for 5 v/v% TCE concentration, whereas it was 0.1 in the H_2SO_4 medium for the same concentration. A higher pitting index value denotes higher corrosion inhibition. From the pitting index values for blank and inhibited metal, it can be said that TCE can be acted as an inhibitor for mild steel in acid media.

3.4. Surface morphological studies

3.4.1. SEM analysis

The interaction mechanism between TCE molecules and mild steel can be substantiated using SEM studies of metal coupons [54]. Fig. S12a reveals the SEM image of the smoothened surface of mild steel. SEM images of the surface of mild steel in 1 M HCl (Fig. S12b and c) and 0.5 M H_2SO_4 (Fig. S12d and e) were presented in the absence and presence of TCE, respectively. It showed that the lack of TCE severely damaged the surface of the mild steel. It was also noticed that the metal destruction is predominant in the 0.5 M H_2SO_4 solution than in 1 M HCl solution. The metal surface became more refined and smooth in the presence of TCE molecules. Therefore, it can be established that TCE behaves as an efficient corrosion inhibitor in acidic media.

3.4.2. AFM analysis

The surface mechanism of TCE on mild steel was further strengthened by AFM analysis. 3-D topography of smoothened metal, blank, metal coupons treated with 5 v/v% TCE in 1 M HCl and 0.5 M H_2SO_4 for 24 h is exhibited in Fig. 7a–e. Surface roughness parameters such as average roughness (R_a), root mean square roughness (R_q), and maximum peak-to-peak height (R_{pp}), which specify the topography of surfaces, are provided in Table 8. On analyzing the table, it can be seen that surface roughness parameters for the smoothened metal were low, whereas those for the metal treated with 1 M HCl and 0.5 M H_2SO_4 were boosted because of the contact with aggressive media. Roughness parameters of the metal surface with TCE were in between that of smoothened and blank metals. It reinforces the adsorption of inhibitor molecules on the metal surface in the corrosion reaction [55]. It was also noticed that the roughness parameters for the metal with TCE in 1 M HCl were lower than those in 0.5 M H_2SO_4, implying that the former medium supports the mitigation of corrosion than the latter.

3.5. Quantum chemical calculations

Quantum chemical parameters of tinosponone and protonated tinosponone such as energy values of HOMO and LUMO, ΔE, ionization energy (I), electron affinity (A), chemical potential (μ), electronegativity (χ), chemical hardness (η), number of electrons transferred (ΔN) are computed in Table 9. The optimized geometry and corresponding HOMO and LUMO of tinosponone and protonated tinosponone are pictured in Fig. 8. Formation of the adsorption layer on the mild steel surface by the donation of electrons can be demonstrated by the value of change in energy (E_{LUMO}–E_{HOMO}). The ΔE value for tinosponone and its protonated form (4.178 and 4.162 eV) enables the shifting of electrons from HOMO of the inhibitor to the vacant orbitals of Fe. It makes TCE an excellent metal protection inhibitor. A value of ΔN less than 3.6 points out a strong propensity for inhibitor molecules to supply electrons to the metal surface [56]. The ΔN value for tinosponone and its protonated form was found to be 1.4265 and 1.4279, respectively, which may be ascribed to the excellent corrosion

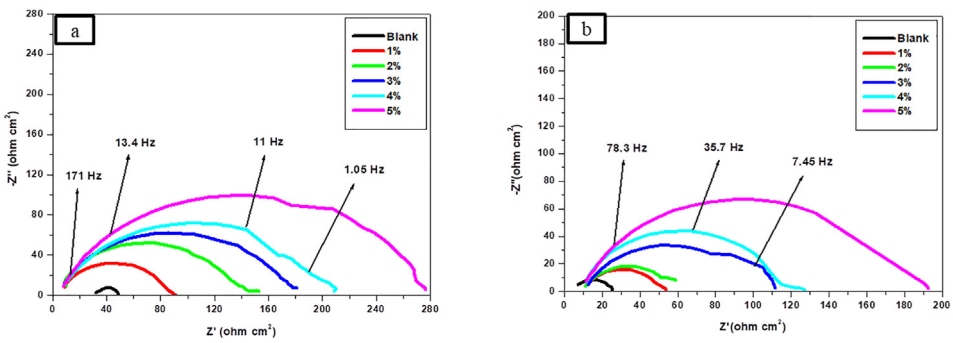

Fig. 4. Nyquist plots of mild steel with varying concentrations of TCE in (a) 1 M HCl and (b) 0.5 M H_2SO_4.

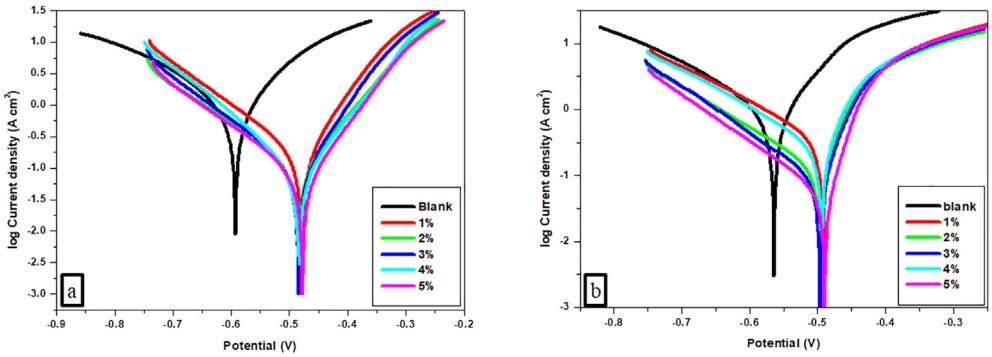

Fig. 5. Tafel plots of mild steel with and without TCE in (a) 1 M HCl and (b) 0.5 M H_2SO_4.

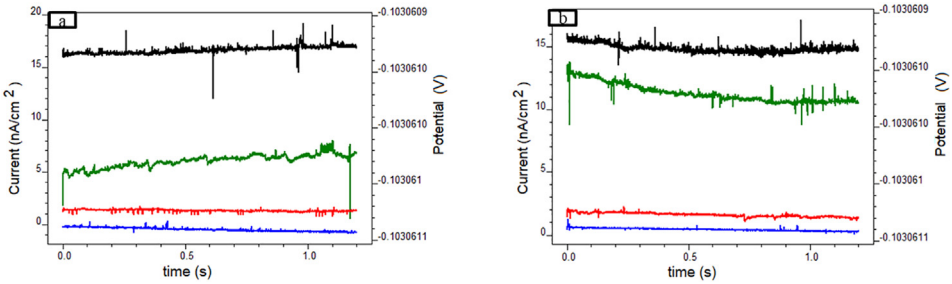

Fig. 6. Current noise for mild steel with and without TCE in (a) 1 M HCl and (b) 0.5 M H_2SO_4.

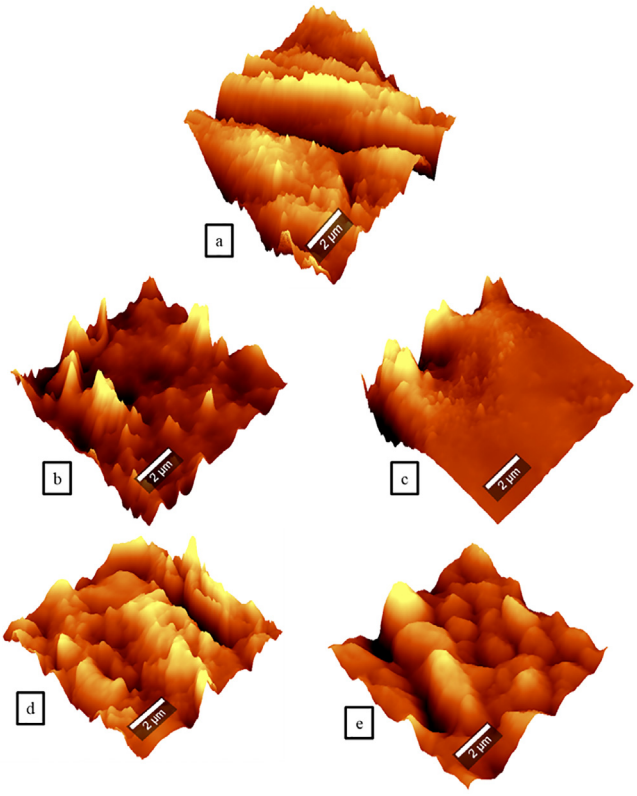

Fig. 7. Topography of mild steel (a) smoothened, (b) in 1 M HCl, (c) in 1 M HCl with 5 v/v% TCE, (d) in 0.5 M H_2SO_4, and (e) in 0.5 M H_2SO_4 with 5 v/v% TCE.

Table 8
Surface roughness parameters of mild steel by AFM analysis.

Metal surface	R_{pp} (nm)	R_q (nm)	R_a (nm)
Smoothened metal	205.27	32.92	26.11
Metal in 1 M HCl	965.86	79.50	55.07
Metal in 1 M HCl with 5 v/v% TCE	646.53	51.65	29.57
Metal in 0.5 M H_2SO_4	2,176.62	231.72	180.48
Metal in 0.5 M H_2SO_4 with 5 v/v% TCE	1,687.53	177.35	142.65

control of TCE. Therefore, theoretical calculations were in line with experimental results.

Monte Carlo simulation (Fig. 9 and Fig. S13) depicts the side view and top view of minor energy adsorption configuration for a tinosponone molecule on Fe (1 1 0) surface as well as for its protonated form. The tinosponone molecule and its protonated form appear fairly adsorbed on the Fe surface. This approach of adsorption may be assigned to the strong interaction between tinosponone and the metal surface. Table 10 represents various energy forms provided in Monte Carlo simulation studies. The summation of energies of the adsorbate, rigid adsorption energy, and deformation energy yields the total energy. Energy of iron surface is considered as zero. When the relaxed adsorbate molecule adsorbed on the iron surface, the releasing/required energy is known as adsorption energy shown in kcal/mol unit, or it can be said that a total of rigid adsorption energy and deformation energy for the adsorbate molecule gives adsorption energy. The rigid adsorption energy means the energy released/required before the geometry optimization step. Simply, when the unrelaxed adsorbate molecule is adsorbed on the iron surface, the resulting energy is known as rigid adsorption energy. The energy released when the adsorbed adsorbate molecule is relaxed on the Fe surface is called

Table 9
Quantum chemical parameters of tinosponone and its protonated form.

Molecule	E_{HOMO} (eV)	E_{LUMO} (eV)	ΔE (eV)	I (eV)	A (eV)	μ (eV)	χ (eV)	η (eV)	ΔN
Tinosponone	−3.129	1.049	4.178	3.129	−1.049	−1.04	1.04	2.089	1.4265
Protonated tinosponone	−3.138	1.024	4.162	3.138	−1.024	−1.057	1.057	2.081	1.4279

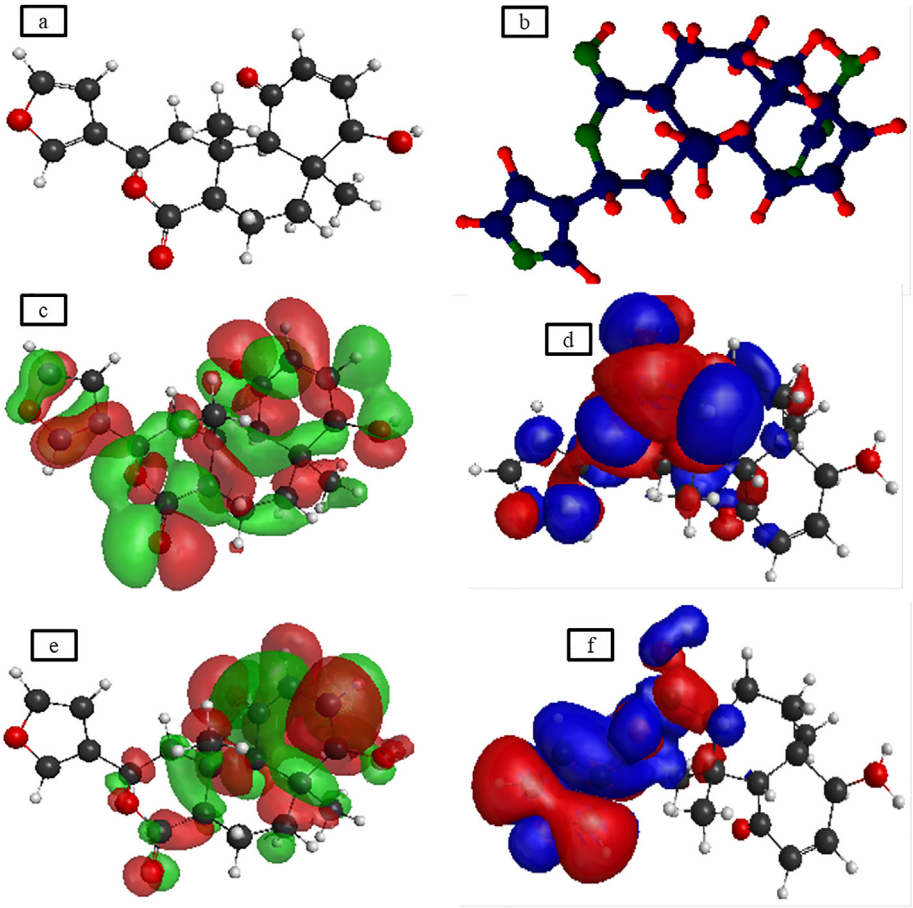

Fig. 8. Optimized geometry of (a) tinosponone and (b) protonated tinosponone; HOMO of (c) tinosponone and (d) protonated tinosponone; LUMO of (e) tinosponone and (f) protonated tinosponone

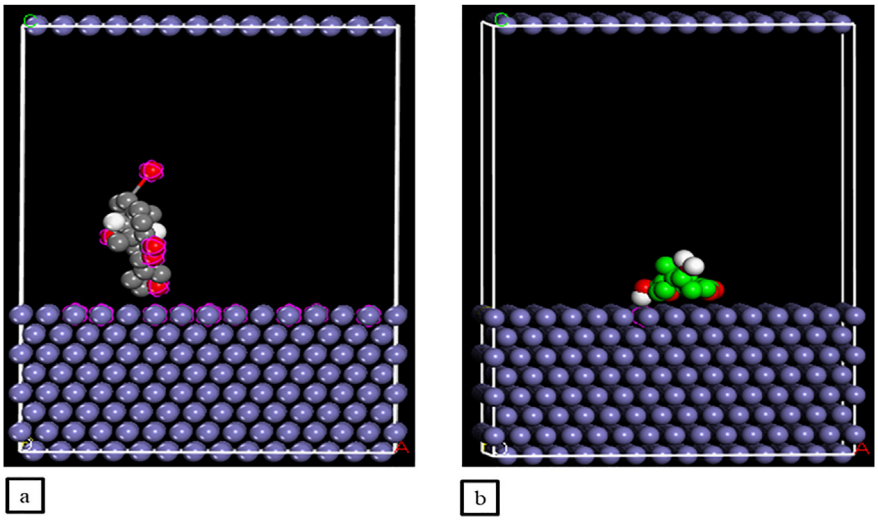

Fig. 9. Equilibrium adsorption configuration of (a) tinosponone and (b) protonated tinosponone on Fe (110) surface from molecular dynamics simulation; front view.

Table 10
Various adsorption structures and the corresponding adsorption energy.

Structure	Total energy (kcal/mol)	Adsorption energy (kcal/mol)	Rigid adsorption energy (kcal/mol)	Deformation energy (kcal/mol)	dE_{ad}/dN_i (kcal/mol)
Tinosponone	10.1254				
Fe surface−tinosponone	−97.8691	−487.2830	−123.5691	−363.7139	−487.2830
Protonated tinosponone	12.3485				
Fe surface−protonated tinosponone	−96.7788	−228.7749	−109.6516	−119.1233	−228.775

deformation energy. Moreover, dE_{ads}/dN_i indicates another form of energy where the adsorbate has been removed. The binding energy was calculated as −107.9945 and −109.1274 kcal/mol for tinosponone and protonated tinosponone, respectively. The negative sign and apparent magnitude recommend a stable adsorption structure of tinosponone on Fe surface. In addition, the negative values of adsorption energy reflect the binding ability of tinosponone and its protonated form with Fe surface [57].

3.6. Statistical analysis

3.6.1. Optimization of factors for IE

Screening experiments revealed that temperature, TCE concentration, and acid concentration significantly influenced the corrosion IE. Therefore, they were selected as independent factors in this study. Weight loss studies showed that the corrosion rate was upgraded in H_2SO_4 medium than in HCl medium. That prompted us to select the HCl solution as an acid medium. The structure of the design and the three levels depending on the BBD of test factors are shown in Table 11, comprising experimental results and predicted response. A total of 15 experimental runs were obtained in it. It was demonstrated that corrosion IE increased with an increase in TCE concentration. This analysis reached maximum efficiency with 5 v/v% TCE concentration in 0.5 M HCl concentration at 313 K. To explore the exact combination of the three factors under study for attaining the immense efficiency, RSM was applied for the optimization technique. The regression model between the test factors and the IE was created at that point, shown in equation (15). Inhibitor efficiency was designated as a function of the test factors in the selected levels using the quadratic equation (15).

$$IE = 5891 - 34.44X_1 + 30.3X_2 - 264.1X_3 + 0.0503X_1^2 - 1.387X_2^2 - 20.79X_3^2 + 0.922X_1X_3 - 1.62X_2X_3 - 0.0397X_1X_2 \quad (15)$$

Table 11
Experimental and predicted inhibition efficiency from weight loss measurements and the BBD.

Run order	Actual level of factors			Inhibition efficiency (%)		Residual (%)
	X_1	X_2	X_3	Experimental	Predicted	
1	313	1	1	60.11293	57.7645	2.34843
2	333	1	1	35.54071	36.4269	0.88619
3	313	5	1	90.39050	89.5043	0.88619
4	333	5	1	62.64005	64.9884	2.34835
5	313	3	0.5	84.60215	84.8844	0.28225
6	333	3	0.5	55.68507	52.7327	2.95237
7	313	3	1.5	60.13363	63.0860	2.95237
8	333	3	1.5	49.66637	49.3841	0.28226
9	323	1	0.5	39.46750	41.5337	2.06620
10	323	5	0.5	74.32543	74.9294	0.60397
11	323	1	1.5	32.80916	32.2052	0.60396
12	323	5	1.5	61.17699	59.1108	2.06619
13	323	3	1	62.68992	62.6899	0.00001
14	323	3	1	62.68992	62.6899	0.00001
15	323	3	1	62.68992	62.6899	0.00001

Table 12
Analysis of variance for corrosion inhibition efficiency.

Source	DF	Adj SS	Adj MS	F-value	*p*-Value
Model	9	3,607.35	400.82	50.79	0.000
Linear	3	3,185.58	1,061.86	134.55	0.000
Temp	1	1,051.27	1,051.27	133.21	0.000
TCE Conc.	1	1,818.13	1,818.13	230.37	0.000
Acid Conc.	1	316.19	316.19	40.06	0.001
Square	3	323.62	107.87	13.67	0.008
Temp*Temp	1	93.38	93.38	11.83	0.018
TCE Conc.*TCE Conc.	1	113.65	113.65	14.40	0.013
Acid Conc.*acid Conc.	1	99.73	99.73	12.64	0.016
2-way interaction	3	98.15	32.72	4.15	0.080
Temp*TCE Conc.	1	2.53	2.53	0.32	0.596
Temp*acid Conc.	1	85.10	85.10	10.78	0.022
TCE Conc.*acid Conc.	1	10.53	10.53	1.33	0.300
Error	5	39.46	7.89		
Lack-of-fit	3	39.46	13.15	*	*
Pure error	2	0.00	0.00		
Total	14	3,646.81			

DF: degrees of freedom, Adj SS: adjusted sum of squares, Adj MS: adjusted mean of squares, *p*: probability.

Using this regression model, analysis of variance (ANOVA) was then applied. ANOVA results with a significance level of 95% are illustrated in Table 12. The most demanding parameter is the *p*-value in this Table. The *p*-value determined the significance of the impact of a factor on response. The degree of essentialness (α) was chosen to be 0.05. It showed that the value of *p* was lower than 0.05 for the linear and square terms. When analyzing the ANOVA results, it explained that TCE concentration was the factor having a significant influence on the response. The Pareto chart (Fig. S14) describes that three linear terms such as temperature, TCE concentration, and acid concentration have an appreciable impact on the IE in which TCE concentration has the most. Squared terms of temperature, TCE concentration, and acid concentration were found to have a low influence on the IE (IE%). The two-way interaction term between factors (X_1X_3) also exhibited a small impact on IE%, whereas the remaining interaction terms (X_1X_2 and X_2X_3) did not reveal any impact on the IE. It is evident from the Pareto chart that TCE concentration is the predominant factor that depends on IE.

The better fit model for experimental results was indicated by the closeness of R^2 and R^2(adj) value to unity [58]. Here, the R^2 and R^2(adj) values were 0.9892 and 0.9697, respectively, indicating the best fit predicted model for experimental values. Therefore, the outcomes can be quickly evaluated by the model.

Main effect plots supplement the outcomes obtained from the regression analysis. It represents how to control tested factors that influence the response [23]. Fig. S15 explains the main effect plots for the fitted means of IE. It showed that the maximum IE was observed for 5 v/v% concentration of TCE at an operating temperature of 313 K at 0.5 M concentration of HCl. Rise in temperature causes a hike in the kinetic energy of the inhibitor molecules and the speed of collision between the molecules. This hinders and destroys the development of adsorbed film inhibitors on the metal

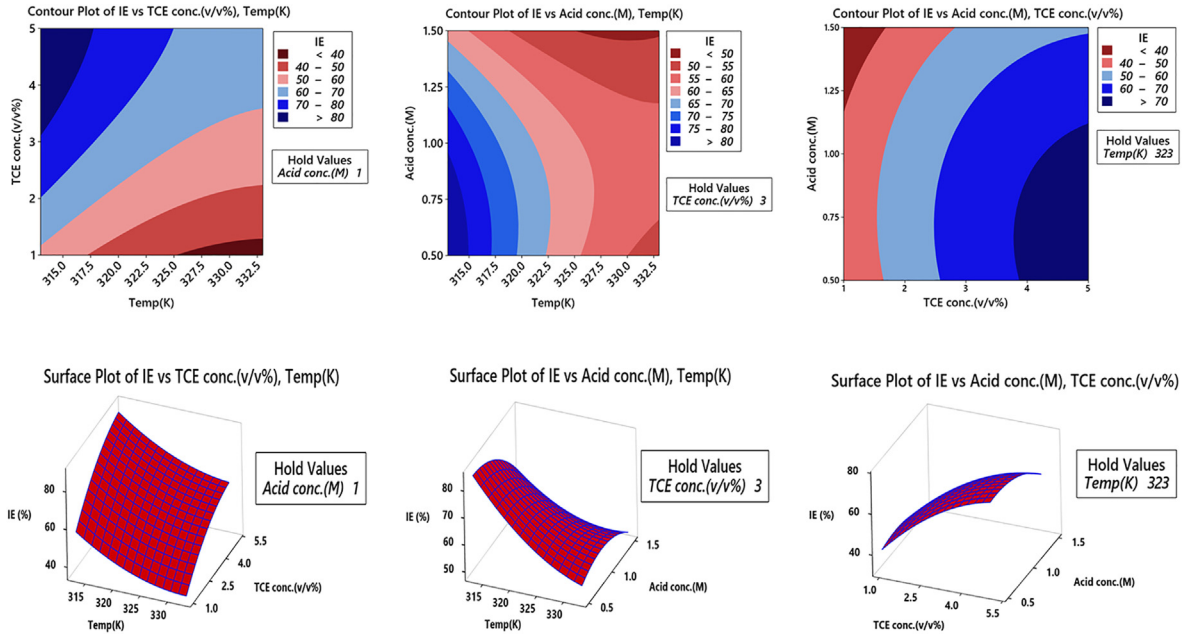

Fig. 10. 3-D contours and surface plots for inhibition efficiency.

surface. Therefore, when the temperature goes up, IE decreases. A close tendency was examined with the concentration of HCl as it was raised from 0.5 M to 1.5 M. As the concentration of the aggressive medium increases, the extent of metal corrosion also increases.

In comparison, the inhibition power of TCE augmented when its concentration was increased from 1 to 5 v/v%. The corrosion rate was much boosted in the absence of an inhibitor and reduced when the inhibitor was present. Thereby adsorption of inhibitor molecules enhances, and efficiency also increases. In summary, temperature and acid concentration offer a negative impact, whereas TCE concentration positively impacts IE.

If the change in response is disparate for two factors, there will be an interaction between them. Fig. S16 exhibits the interaction plot for IE. Crossed lines in the interaction plot indicate a significant interaction between the factors, whereas parallel or straight lines point out little interaction. From Fig. S16, it was examined that the two-way interaction terms were trivial as there are no crossed lines except in the temp-acid concentration two-way interaction term (X_1X_3). Outcomes of ANOVA analysis also revealed that the *p*-value was higher than 0.05 for two-way interactions, and only one interaction term has a lower *p*-value, i.e. X_1X_3. Therefore, two-way interaction terms do not have any significant impact on IE.

3-D contours and surface plots demonstrate the interdependence of the tested factors on IE (%) and are presented in Fig. 10 [59]. It was exhibited that the IE goes up when TCE concentration rises for a given temperature. However, IE and temperature have a reverse relationship. This trend can be ascribed to the physical adsorption of TCE molecules on the mild steel surface. Similarly, IE and acid concentration are inversely proportional.

3.6.2. Response optimization

A well-organized numerical model in equation (15) was used with the goal of optimizing the independent variables such as temperature, TCE concentration, and acid concentration to bring about the maximum IE. For the most remarkable and feasible response, the desirability function method was used by improving tested factors. The response optimization plot for IE is shown in Fig. S17. The anticipated optimum factors identified were temperature of 313 K, TCE concentration of 5 v/v%, and acid concentration of 0.5 M for the HCl environment. The corresponding predicted IE was 96.82%, as depicted in Fig. S17. Experimental results were in exact agreement with statistical analysis. Confirmation tests achieved validation of the optimal factor settings and the amelioration of the IE. Confirmation tests also helped verify the recurrence of the experimental outcomes and approve the prescient model's accuracy.

4. Conclusions

Toxicity and non-biodegradability are two crucial problems of corrosion inhibitors. The present work has investigated *Tinospora cordifolia* plant leaf extract as an eco-friendly corrosion inhibitor for mild steel in 1 M HCl and 0.5 M H_2SO_4 media.

- Weight loss measurements showed excellent TCE performance in mitigating mild steel corrosion in 1 M HCl compared with 0.5 M H_2SO_4. An increase in TCE concentration results in improved inhibition power. As per weight loss measurements, when temperature increased to 333 K, a decrease in TCE inhibition was observed. The maximum inhibition potency of TCE in 1 M HCl and 0.5 M H_2SO_4 was calculated as 94.73% and 82.53%, respectively.
- Electrochemical studies go along with weight loss measurements. TCE acted as a mixed-type inhibitor from potentiodynamic polarization techniques as it simultaneously restrains the anodic and cathodic reactions of mild steel.
- The Langmuir adsorption isotherm was reckoned to be good adsorption of TCE molecules on mild steel surface in both acid media. ΔG^0_{ads} values (−30.37 and −27.15 kJ/mol) obtained from adsorption studies revealed that the adsorption is by physisorption and chemisorption.
- Surface morphological studies furnish strong proof for developing a protective film on mild steel with TCE in acidic media.
- As per quantum chemical investigations, the presence of tinosponone molecules in TCE greatly favors electron donation from

HOMO of the inhibitor to LUMO of metal having a low ΔE value (4.178 eV).
- The regression model could describe the interdependence between factors on the IE and the results obtained from experiments in good agreement.

These observations provide appropriate verification for using TCE as an eco-friendly and renewable corrosion inhibitor in acid media.

Credit author statement

Vidhya Thomas K: Conceptualization, Methodology, Writing – original draft; **Joby Thomas K:** Supervision; **Vinod P Raphael:** Validation; **AS Sabu:** Software; **Ragi K:** Writing – review & editing; **Reeja Johnson:** Reviewing.

Declaration of competing interest

The authors declare that they have no known competing financial interests or personal relationships that could have appeared to influence the work reported in this paper.

Appendix A. Supplementary data

Supplementary data to this article can be found online at https://doi.org/10.1016/j.mtsust.2021.100076.

References

[1] Z.P. Mathew, K. Rajan, C. Augustine, B. Joseph, S. John, Corrosion inhibition of mild steel using poly (2-ethyl -2-oxazoline) in 0.1M HCl solution, Heliyon 6 (2020), e05560, https://doi.org/10.1016/j.heliyon.2020.e05560.

[2] S. Hooshmand Zaferani, M. Sharifi, D. Zaarei, M.R. Shishesaz, Application of eco-friendly products as corrosion inhibitors for metals in acid pickling processes – a review, J. Environ. Chem. Eng. 1 (2013) 652–657, https://doi.org/10.1016/j.jece.2013.09.019.

[3] S.S. de Assunção Araújo Pereira, M.M. Pêgas, T.L. Fernández, M. Magalhães, T.G. Schöntag, D.C. Lago, L.F. de Senna, E. D'Elia, Inhibitory action of aqueous garlic peel extract on the corrosion of carbon steel in HCl solution, Corrosion Sci. 65 (2012) 360–366, https://doi.org/10.1016/j.corsci.2012.08.038.

[4] K.K. Anupama, K. Ramya, K.M. Shainy, A. Joseph, Adsorption and electrochemical studies of Pimenta dioica leaf extracts as corrosion inhibitor for mild steel in hydrochloric acid, Mater. Chem. Phys. 167 (2015) 28–41, https://doi.org/10.1016/j.matchemphys.2015.09.013.

[5] A.A. Ayoola, O.S.I. Fayomi, I.G. Akande, O.A. Ayeni, O. Agboola, O.R. Obanla, O.G. Abatan, C.J. Chukwuka, Inhibitive corrosion performance of the eco-friendly aloe vera in acidic media of mild and stainless steels, J. Bio- Tribo-Corrosion 6 (2020) 1–13, https://doi.org/10.1007/s40735-020-00361-y.

[6] D. Li, P. Zhang, X. Guo, X. Zhao, Y. Xu, The inhibition of mild steel corrosion in 0.5 M H_2SO_4 solution by radish leaf extract, RSC Adv. 9 (2019) 40997–41009, https://doi.org/10.1039/c9ra04218k.

[7] A. Jmiai, B. El Ibrahimi, A. Tara, M. Chadili, S. El Issami, O. Jbara, A. Khallaayoun, L. Bazzi, Application of Zizyphus Lotuse – pulp of Jujube extract as green and promising corrosion inhibitor for copper in acidic medium, J. Mol. Liq. 268 (2018) 102–113, https://doi.org/10.1016/j.molliq.2018.06.091.

[8] A. Saxena, V. Sharma, K.K. Thakur, N. Bhardwaj, Electrochemical studies and the surface examination of low carbon steel by applying the extract of Citrus sinensis, J. Bio- Tribo-Corrosion 6 (2020), https://doi.org/10.1007/s40735-020-00338-x.

[9] A.Y. El-Etre, M. Abdallah, Z.E. El-Tantawy, Corrosion inhibition of some metals using lawsonia extract, Corrosion Sci. 47 (2005) 385–395, https://doi.org/10.1016/j.corsci.2004.06.006.

[10] A.Y. El-Etre, Inhibition of acid corrosion of carbon steel using aqueous extract of olive leaves, J. Colloid Interface Sci. 314 (2007) 578–583, https://doi.org/10.1016/j.jcis.2007.05.077.

[11] M. Shyamala, A. Arulanantham, Eclipta alba as corrosion pickling inhibitor on mild steel in hydrochloric acid, J. Mater. Sci. Technol. -Shenyang- 25 (2009).

[12] A.M. Abdel-Gaber, H.T. Rahal, F.T. Beqai, Eucalyptus leaf extract as a eco-friendly corrosion inhibitor for mild steel in sulfuric and phosphoric acid solutions, Int. J. Ind. Chem. 11 (2020) 123–132, https://doi.org/10.1007/s40090-020-00207-z.

[13] Z. Sanaei, M. Ramezanzadeh, G. Bahlakeh, B. Ramezanzadeh, Use of Rosa canina fruit extract as a green corrosion inhibitor for mild steel in 1M HCl solution: a complementary experimental, molecular dynamics and quantum mechanics investigation, J. Ind. Eng. Chem. 69 (2019) 18–31, https://doi.org/10.1016/j.jiec.2018.09.013.

[14] Q. Wang, B. Tan, H. Bao, Y. Xie, Y. Mou, P. Li, D. Chen, Y. Shi, X. Li, W. Yang, Evaluation of Ficus tikoua leaves extract as an eco-friendly corrosion inhibitor for carbon steel in HCl media, Bioelectrochemistry 128 (2019) 49–55, https://doi.org/10.1016/j.bioelechem.2019.03.001.

[15] M. Ramezanzadeh Karati, G. Bahlakeh, Z. Sanaei, B. Ramezanzadeh, Corrosion inhibition of mild steel in 1 M HCl solution by ethanolic extract of eco-friendly Mangifera indica (mango) leaves: electrochemical, molecular dynamics, Monte Carlo and ab initio study, Appl. Surf. Sci. 463 (2018), https://doi.org/10.1016/j.apsusc.2018.09.029.

[16] M.T. Majd, M. Ramezanzadeh, B. Ramezanzadeh, G. Bahlakeh, Production of an environmentally stable anti-corrosion film based on Esfand seed extract molecules-metal cations: integrated experimental and computer modeling approaches, J. Hazard. Mater. 382 (2020) 121029, https://doi.org/10.1016/j.jhazmat.2019.121029.

[17] N.K. Othman, S. Yahya, M.C. Ismail, Corrosion inhibition of steel in 3.5% NaCl by rice straw extract, J. Ind. Eng. Chem. 70 (2019) 299–310, https://doi.org/10.1016/j.jiec.2018.10.030.

[18] B. Tan, B. Xiang, S. Zhang, Y. Qiang, L. Xu, S. Chen, J. He, Papaya leaves extract as a novel eco-friendly corrosion inhibitor for Cu in H_2SO_4 medium, J. Colloid Interface Sci. 582 (2021) 918–931, https://doi.org/10.1016/j.jcis.2020.08.093.

[19] M.T. majd, M. Ramezanzadeh, G. Bahlakeh, B. Ramezanzadeh, Probing molecular adsorption/interactions and anti-corrosion performance of poppy extract in acidic environments, J. Mol. Liq. 304 (2020) 112750, https://doi.org/10.1016/j.molliq.2020.112750.

[20] A. Dehghani, G. Bahlakeh, B. Ramezanzadeh, M. Ramezanzadeh, A combined experimental and theoretical study of green corrosion inhibition of mild steel in HCl solution by aqueous Citrullus lanatus fruit (CLF) extract, J. Mol. Liq. 279 (2019) 603–624, https://doi.org/10.1016/j.molliq.2019.02.010.

[21] S.A. Haddadi, E. Alibakhshi, G. Bahlakeh, B. Ramezanzadeh, M. Mahdavian, A detailed atomic level computational and electrochemical exploration of the Juglans regia green fruit shell extract as a sustainable and highly efficient green corrosion inhibitor for mild steel in 3.5 wt% NaCl solution, J. Mol. Liq. 284 (2019) 682–699, https://doi.org/10.1016/j.molliq.2019.04.045.

[22] D. Prabhu, P.R. Prabhu, P. Rao, Thermodynamics, adsorption, and response surface methodology investigation of the corrosion inhibition of aluminum by Terminalia chebula Ritz. extract in H_3PO_4, Chem. Pap. (2020), https://doi.org/10.1007/s11696-020-01318-8.

[23] P.R. Prabhu, D. Prabhu, P. Rao, Analysis of Garcinia indica Choisy extract as eco-friendly corrosion inhibitor for aluminum in phosphoric acid using the design of experiment, J. Mater. Res. Technol. 9 (2020) 3622–3631, https://doi.org/10.1016/j.jmrt.2020.01.100.

[24] V.C. Anadebe, O.D. Onukwuli, M. Omotioma, N.A. Okafor, Optimization and electrochemical study on the control of mild steel corrosion in hydrochloric acid solution with bitter kola leaf extract as inhibitor, S. Afr. J. Chem. 71 (2018) 51–61, https://doi.org/10.17159/0379-4350/2018/v71a7.

[25] S.S. Singh, S.C. Pandey, S. Srivastava, V.S. Gupta, B. Patro, A.C. Ghosh, Chemistry and medicinal properties of Tinospora cordifolia (Guduchi), Indian J. Pharmacol. 35 (2003) 83–91.

[26] K.K. Reddi, S.D. Tetali, Dry leaf extracts of Tinospora cordifolia (Willd.) Miers attenuate oxidative stress and inflammatory condition in human monocytic (THP-1) cells, Phytomedicine 61 (2019) 152831, https://doi.org/10.1016/j.phymed.2019.152831.

[27] M.P. Binsi, T.K. Joby, K. Ragi, V.C. Sini, J. Reeja, Interaction of two heterocyclic schiff bases derived from 2-acetyl pyridine on mild steel in hydrochloric acid: physicochemical and corrosion inhibition investigations, Curr. Chem. Lett. 9 (2020) 19–30, https://doi.org/10.5267/j.ccl.2019.006.005.

[28] P. Mourya Savita, N. Chaubey, S. Kumar, V.K. Singh, M.M. Singh, Strychnos nuxvomica, Piper longum and Mucuna pruriens seed extracts as eco-friendly corrosion inhibitors for copper in nitric acid, RSC Adv. 6 (2016) 95644–95655, https://doi.org/10.1039/C6RA16481A.

[29] K. Shainy, K. Anupama, A. Joseph, Excellent anticorrosion behavior of Ruta graveolens extract (RGE) for mild steel in hydrochloric acid: electro analytical studies on the effect of time , temperature , and inhibitor concentration, J. Bio- Tribo-Corrosion 2 (2016) 1–10, https://doi.org/10.1007/s40735-016-0032-5.

[30] S.C. Udensi, O.E. Ekpe, L.A. Nnanna, Newbouldia laevis leaves extract as tenable eco-friendly corrosion inhibitor for aluminium alloy AA7075-T7351 in 1 M HCl corrosive environment: gravimetric, electrochemical and thermodynamic studies, Chem. Afr. 3 (2020) 303–316, https://doi.org/10.1007/s42250-020-00131-w.

[31] V.P. Raphael, J.T. Kakkassery, S.K. Shanmughan, S. Varghese, Interaction of two water soluble heterocyclic hydrazones on copper in nitric acid: electrochemical, surface morphological, and quantum chemical investigations, Int. J. Met. 2016 (2016) 1–8, https://doi.org/10.1155/2016/6509469.

[32] K.K. Anupama, A. Joseph, Experimental and theoretical studies on Cinnamomum verum leaf extract and one of its major components, eugenol as environmentally benign corrosion inhibitors for mild steel in acid media, J. Bio-Tribo-Corrosion 4 (2018), https://doi.org/10.1007/s40735-018-0146-z.

[33] O. Sanni, A.P.I. Popoola, Assessment of concentration, temperature and exposure time effect on waste product as a sustainable inhibitor for stainless steel corrosion: optimization using response surface method, J. Bio- Tribo-Corrosion 5 (2019) 1–14, https://doi.org/10.1007/s40735-019-0239-3.

[34] A. Dehghani, G. Bahlakeh, B. Ramezanzadeh, M. Ramezanzadeh, Experimental complemented with microscopic (electronic/atomic)-level modeling explorations of Laurus nobilis extract as green inhibitor for carbon steel in acidic solution, J. Ind. Eng. Chem. 84 (2020) 52–71, https://doi.org/10.1016/j.jiec.2019.12.019.
[35] S. Chen, B. Zhu, X. Liang, Corrosion inhibition performance of coconut leaf extract as a green corrosion inhibitor for X65 steel in hydrochloric acid solution, Int. J. Electrochem. Sci. 15 (2020) 1–15, https://doi.org/10.20964/2020.01.39.
[36] S. Chen, S. Chen, B. Zhu, C. Huang, W. Li, Magnolia grandiflora leaves extract as a novel environmentally friendly inhibitor for Q235 steel corrosion in 1 M HCl: combining experimental and theoretical researches, J. Mol. Liq. 311 (2020) 113312, https://doi.org/10.1016/j.molliq.2020.113312.
[37] S. Chen, H. Zhao, S. Chen, P. Wen, H. Wang, W. Li, Camphor leaves extract as a neoteric and environment friendly inhibitor for Q235 steel in HCl medium: combining experimental and theoretical researches, J. Mol. Liq. 312 (2020) 113433, https://doi.org/10.1016/j.molliq.2020.113433.
[38] R. Kooliyat, J.T. Kakkassery, V.P. Raphael, S.V. Cheruvathur, B.M. Paulson, Synthesis, cyclic voltammetric, electrochemical, and gravimetric corrosion inhibition investigations of schiff base derived from 5,5-Dimethyl-1,3-cyclohexanedione and 2-aminophenol on mild steel in 1 M HCl and 0.5 M H_2SO_4, Int. J. Electrochem. 2019 (2019) 1–13, https://doi.org/10.1155/2019/1094148.
[39] J. Aljourani, M.A. Golozar, K. Raeissi, The inhibition of carbon steel corrosion in hydrochloric and sulfuric acid media using some benzimidazole derivatives, Mater. Chem. Phys. 121 (2010) 320–325, https://doi.org/10.1016/j.matchemphys.2010.01.040.
[40] K. Muthamma, P. Kumari, M. Lavanya, S.A. Rao, Corrosion inhibition of mild steel in acidic media by N-[(3,4-Dimethoxyphenyl)Methyleneamino]-4-Hydroxy-Benzamide, J. Bio- Tribo-Corrosion 7 (2021) 1–19, https://doi.org/10.1007/s40735-020-00439-7.
[41] M.A. Bidi, M. Azadi, M. Rassouli, A new green inhibitor for lowering the corrosion rate of carbon steel in 1 M HCl solution: Hyalomma tick extract, Mater. Today Commun. 24 (2020) 100996, https://doi.org/10.1016/j.mtcomm.2020.100996.
[42] O.O. Ogunleye, A.O. Arinkoola, O.A. Eletta, O.O. Agbede, Y.A. Osho, A.F. Morakinyo, J.O. Hamed, Green corrosion inhibition and adsorption characteristics of Luffa cylindrica leaf extract on mild steel in hydrochloric acid environment, Heliyon 6 (2020), e03205, https://doi.org/10.1016/j.heliyon.2020.e03205.
[43] M. Erna, H. Herdini, D. Futra, Corrosion inhibition mechanism of mild steel by amylose-acetate/carboxymethyl chitosan composites in acidic media, Int. J. Chem. Eng. 2019 (2019) 8514132, https://doi.org/10.1155/2019/8514132.
[44] O. Dagdag, Z. Safi, H. Erramli, N. Wazzan, L. Guo, C. Verma, E.E. Ebenso, S. Kaya, A. El Harfi, Epoxy prepolymer as a novel anti-corrosive material for carbon steel in acidic solution: electrochemical, surface and computational studies, Mater. Today Commun. 22 (2020), https://doi.org/10.1016/j.mtcomm.2019.100800.
[45] O.A. Akinbulumo, O.J. Odejobi, E.L. Odekanle, Thermodynamics and adsorption study of the corrosion inhibition of mild steel by Euphorbia heterophylla L. extract in 1.5 M HCl, Results Mater. 5 (2020) 100074, https://doi.org/10.1016/j.rinma.2020.100074.
[46] C.M. Fernandes, T. da S. Ferreira Fagundes, N. Escarpini dos Santos, T. Shewry de M. Rocha, R. Garrett, R.M. Borges, G. Muricy, A.L. Valverde, E.A. Ponzio, Ircinia strobilina crude extract as corrosion inhibitor for mild steel in acid medium, Electrochim. Acta 312 (2019) 137–148, https://doi.org/10.1016/j.electacta.2019.04.148.
[47] V.R. Palayoor, J.T. Kakkassery, S.S. Kanimangalath, S. Varghese, Chemical modification at the surface and corrosion inhibition response of two semicarbazones on carbon steel in HCl medium, Int. J. Ind. Chem. 8 (2017) 49–60, https://doi.org/10.1007/s40090-016-0101-0.
[48] K.K. Anupama, K. Ramya, A. Joseph, Electrochemical measurements and theoretical calculations on the inhibitive interaction of Plectranthus amboinicus leaf extract with mild steel in hydrochloric acid, Meas. J. Int. Meas. Confed. 95 (2017) 297–305, https://doi.org/10.1016/j.measurement.2016.10.030.
[49] P. Preethi Kumari, P. Shetty, S.A. Rao, Electrochemical measurements for the corrosion inhibition of mild steel in 1 M hydrochloric acid by using an aromatic hydrazide derivative, Arab. J. Chem. 10 (2017) 653–663, https://doi.org/10.1016/j.arabjc.2014.09.005.
[50] A. Singh, Y. Caihong, Y. Yaocheng, N. Soni, Y. Wu, Y. Lin, Analyses of new electrochemical techniques to study the behavior of some corrosion mitigating polymers on N80 tubing steel, ACS Omega 4 (2019) 3420–3431, https://doi.org/10.1021/acsomega.8b02983.
[51] A. Singh, K.R. Ansari, D.S. Chauhan, M.A. Quraishi, H. Lgaz, I.M. Chung, Comprehensive investigation of steel corrosion inhibition at macro/micro level by ecofriendly green corrosion inhibitor in 15% HCl medium, J. Colloid Interface Sci. 560 (2020) 225–236, https://doi.org/10.1016/j.jcis.2019.10.040.
[52] V.P. Raphael, S.K. Shanmughan, J.T. Kakkassery, Monitoring the interaction of two heterocyclic compounds on carbon steel by electrochemical polarization, noise, and quantum chemical studies, Int. J. Corrosion 2016 (2016) 4204532, https://doi.org/10.1155/2016/4204532.
[53] K. Ragi, J.T. Kakkassery, V.P. Raphael, B.M. Paulson, R. Johnson, Corrosion inhibition of mild steel by N, N′-(5,5-dimethylcyclohexane-1,3-diylidene)dianiline in acid media: gravimetric and electrochemical evaluations, Curr. Chem. Lett. 10 (2021) 67–80, https://doi.org/10.5267/j.ccl.2020.8.001.
[54] A. Saxena, K.K. Thakur, K.K. Saxena, S. Chambyal, A. Sharma, Electrochemical studies and surface examination of low carbon steel by applying the extract of Terminalia chebula, Mater. Today Proc. 26 (2019) 1360–1367, https://doi.org/10.1016/j.matpr.2020.02.276.
[55] R. Haldhar, D. Prasad, A. Saxena, R. Kumar, Experimental and theoretical studies of Ficus religiosa as green corrosion inhibitor for mild steel in 0.5 M H2SO4 solution, Sustain. Chem. Pharm. 9 (2018) 95–105, https://doi.org/10.1016/j.scp.2018.07.002.
[56] A. Farhadian, A. Rahimi, N. Safaei, A. Shaabani, M. Abdouss, A. Alavi, A theoretical and experimental study of castor oil-based inhibitor for corrosion inhibition of mild steel in acidic medium at elevated temperatures, Corrosion Sci. 175 (2020) 108871, https://doi.org/10.1016/j.corsci.2020.108871.
[57] N. Asadi, M. Ramezanzadeh, G. Bahlakeh, B. Ramezanzadeh, Utilizing Lemon Balm extract as an effective green corrosion inhibitor for mild steel in 1M HCl solution: a detailed experimental, molecular dynamics, Monte Carlo and quantum mechanics study, J. Taiwan Inst. Chem. Eng. 95 (2019) 252–272, https://doi.org/10.1016/j.jtice.2018.07.011.
[58] A.S. Sabu, A. Mathew, T.S. Neethu, K. Anil George, Statistical analysis of MHD convective ferro-nanofluid flow through an inclined channel with hall current, heat source and soret effect, Therm. Sci. Eng. Prog. 22 (2021) 100816, https://doi.org/10.1016/j.tsep.2020.100816.
[59] Y.P. Asmara, Athirah, J.P. Siregar, T. Kurniawan, D. Bachtiar, Application of response surface methodology method in designing corrosion inhibitor, IOP Conf. Ser. Mater. Sci. Eng. 257 (2017), https://doi.org/10.1088/1757-899X/257/1/012090.